
Article:
Halcrow, MA orcid.org/0000-0001-7491-9034, Capel Berdiell, I, Pask, CM orcid.org/0000-0002-2241-5069 et al. (1 more author) (2019) Relationship between the Molecular Structure and Switching Temperature in a Library of Spin-Crossover Molecular Materials. Inorganic Chemistry, 58 (15). pp. 9811-9821. ISSN 0020-1669

https://doi.org/10.1021/acs.inorgchem.9b00843

The Relationship Between Molecular Structure and Switching Temperature in a Library of Spin-Crossover Molecular Materials

Malcolm A. Halcrow,[†,] Izar Capel Berdiell[†], Christopher M. Pask[†] and Rafal Kulmaczewski[†]*

[†]School of Chemistry, University of Leeds, Woodhouse Lane, Leeds LS2 9JT, UK.

ABSTRACT

Structure:function relationships are surveyed relating the spin-crossover (SCO) midpoint temperature ($T_{½}$) in the solid state, for 43 members of the iron(II)/dipyrazolylpyridine family of SCO compounds. The difference between $T_{½}$ in the solid state and in solution [ΔT(latt)] is proposed as a measure of the lattice contribution to the transition temperature. Negative linear correlations between SCO temperature and the magnitude of the rearrangement of the coordination sphere during SCO are evident among isostructural or near-isostructural subsets of compounds; that is, a larger change in molecular structure during SCO stabilizes the high-spin state of a material. Improved correlations are often obtained when ΔT(latt), rather than the raw $T_{½}$ value, is considered as the measure of SCO temperature. Different lattice types show different tendencies to stabilize the high-spin or low-spin state of the molecules containing them, which correlates with the structural changes that most influence ΔT(latt) in each case. These relationships are mostly unaffected by the SCO cooperativity in the compounds, or by the involvement of any crystallographic phase changes. One or two materials within each subset are outliers in some or all of these correlations however which, in some cases, can be attributed to small differences in their ligand geometry or unusual phase behavior during SCO. A re-investigation of the structural chemistry of $[Fe(3\text{-bpp})_2][NCS]_2 \cdot n H_2O$ (3-bpp = di{1*H*-pyrazol-3-yl}pyridine; n = 0 or 2), undertaken as part of this study, is also presented.

.

Introduction

Spin-crossover (SCO) compounds are versatile molecular switches, where a change in metal ion spin state is triggered by a thermal, optical or pressure stimulus.[1,2] This affects the magnetic moment, color, conductivity[3] and dielectric constant[4] of solid SCO compounds, and can also lead to a mechanical response.[5] Multifunctional materials using SCO to modulate fluorescence[6] or a non-linear optical response,[7] or induce single-molecule[8] or bulk magnetic ordering[9] at low temperatures, have also been achieved. Exploitation of these properties in device and nanotechnology applications[2,5] requires an understanding of structure:function relationships in SCO molecular materials.[10] More fundamentally, SCO crystals are also useful models for mechanistic studies of crystallographic phase transitions.[11]

The relationship between molecular structure and crystal packing on one hand, and the temperature and cooperativity of SCO transitions on the other, remains a difficult crystal engineering problem.[10] In that regard, an intriguing structure:function relationship was noted by Guionneau *et al* in 2005, in complexes of the *cis*-[Fe(NCS)$_2$*L*$_2$] type (*L* is a bidentate N-donor ligand). Nine out of eleven complexes in that survey displayed a negative linear relationship between the SCO midpoint temperature ($T_{½}$), and an angular distortion of the coordination geometry (Figure S1).[12] That is, materials whose SCO involves a greater angular rearrangement of their coordination sphere are stabilized in the high-spin form, thus exhibiting a lower $T_{½}$. Although the trend has not yet been addressed computationally, it is reasonable that more anisotropic structural changes during SCO would lead to a higher kinetic barrier for the transition, imposed by the surrounding solid lattice. That higher activation energy would require additional supercooling of the material to induce SCO, as observed.[10,13]

That observation has not yet been generalized to any other class of material. Part of the challenge is that, despite the plethora of SCO complexes known, there are few families of chemically similar and/or isostructural SCO materials that allow individual structure:function trends to be identified. In that regard, the library of compounds related to $[Fe(1\text{-bpp})_2]X_2$ (Chart 1; 1-bpp = 2,6-di{pyrazol-1-yl}pyridine; X^- = a monovalent anion) is a valuable resource. Over 100 such compounds have been published containing 1-bpp or a substituted $bpp^{X,H}$ or $bpp^{H,Y}$ derivative, around half of which are known to be SCO-active in the solid state.[14,15] That number increases further when complexes of the isomeric 3-bpp and 1,3-bpp ligand families are also considered.[16]

Chart 1 $[Fe(1\text{-bpp})_2]X_2$ (top), and the ligand types referred to in this study.

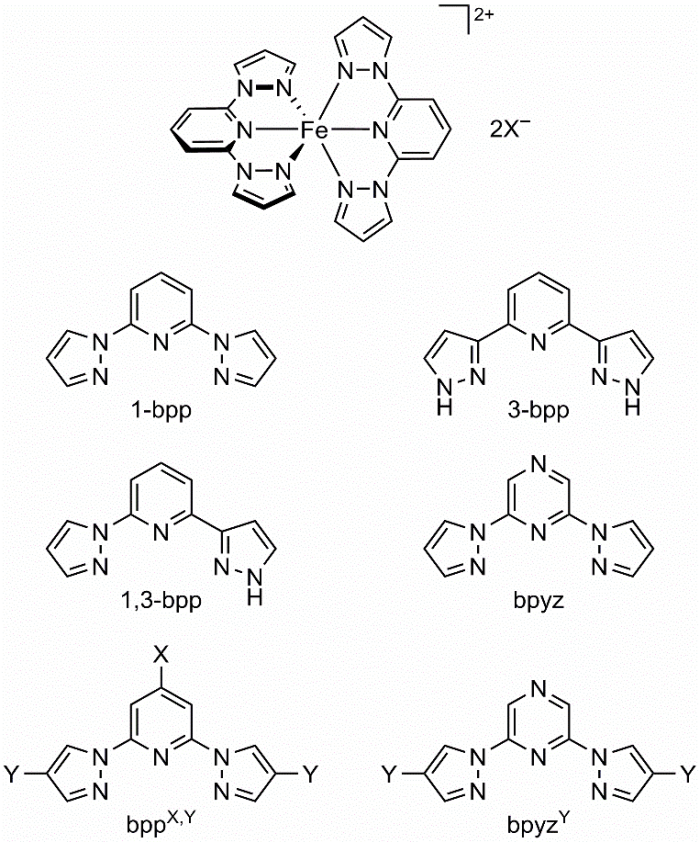

We recently reported a rationalization of the influence of ligand substituents on $T_{½}$ of 26 [Fe(1-bpp)$_2$]X$_2$ derivatives based on solution phase data.[17] A structure:function correlation for $T_{½}$ in the solid state presents additional challenges, where the spin-state of a complex is perturbed by the rigid solid lattice. The chemical pressure exerted on a molecule by its nearest neighbors constrains its geometry, changing the relative enthalpies of the spin states as the transition proceeds.[18] Phonon entropy also contributes to SCO thermodynamics in condensed phases, as a function of the lattice symmetry as well as the intra- and inter-molecular bonding interactions.[19]

We have now applied our data to correlate molecular structure with $T_{½}$ in the solid state, in complexes of these ligand families (Chart 1). The results extend Guionneau *et al.*'s conclusions, while emphasizing that solid state SCO cannot be considered as a purely molecular phenomenon.

Experimental

No new compounds were synthesized during this study. Graph plotting and linear regression fits were carried out with *SIGMAPLOT*,[20] using structural data from our laboratory or from the Cambridge Crystallographic Database.[21]

Previously unpublished solution-phase magnetic data from compounds in our laboratory were obtained by Evans method (Figure S2).[22] Diamagnetic corrections were calculated from Pascal's constants,[23] and a correction for changes to the density of the CD_3CN solvent with temperature was also applied.[24]

Crystallographic and magnetic data from a new anhydrous phase of [Fe(3-bpp)$_2$][NCS]$_2$[25,26] are presented in the Supporting Information. Solid state magnetic measurements were obtained with a Quantum Design SQUID or VSM SQUID magnetometers, in an applied field of 5000 G

with a temperature ramp of 5 K min^{-1}. Diamagnetic corrections for the samples were estimated from Pascal's constants.[23] A diamagnetic correction for the sample holder was measured separately, and also applied to the data.

Results and Discussion

As well as the absolute SCO transition temperature $T_{½}$, the difference in $T_{½}$ between the solid and solution phases [ΔT(latt), eq 1] was also considered as a measure of the lattice contribution to $T_{½}$ in the solid state.

$$\Delta T(\text{latt}) = T_{½}(\text{solid}) - T_{½}(\text{solution}) \quad (1)$$

A positive value of ΔT(latt) indicates the lattice stabilizes the low-spin state and raises $T_{½}$(solid), compared to the same compound in fluid solution. Table 1 lists such complexes whose $T_{½}$(solid) is accurately known; where $T_{½}$(solution) is known, or can be estimated based on a published σ^{+} Hammett parameter;[17] and, where at least one crystal structure is available.

A complication in this definition is that $T_{½}$(solution) for $[Fe(3\text{-bpp})_2]^{2+}$ and $[Fe(1,3\text{-bpp})_2]^{2+}$ is solvent-dependent, reflecting the influence of hydrogen bonding to their distal N–H groups.[27] Thus $[Fe(3\text{-bpp})_2]^{2+}$ exhibits $T_{½}$(solution) ranging from 244 K in $MeNO_2$ to 255 K in dmf,[27] which also increases further in the presence of water.[15,27,28] Similarly, $T_{½}$(solution) for $[Fe(1,3\text{-bpp})_2]^{2+}$ has been measured as 254 K in acetone[15] or 262 K in MeOH.[29] We employed the lower $T_{½}$(solution) values in this analysis, which reflects the hydrophobic lattices in the anhydrous crystals in the Table while also giving the best agreement in the structure:function correlations described below. There is no evidence for a solvent-dependence of $T_{½}$(solution) in $[Fe(1\text{-bpp})_2]^{2+}$ derivatives, which have no hydrogen bond donors in their heterocyclic ligand framework.[17]

Table 1. The compounds considered in this work (Chart 1), with references. The structural parameters that were correlated with these data are listed in Table S2. Compounds in italics are "outliers" in many of the structure:function plots discussed.

	$T_{½}$(solid) / K	$T_{½}$(solution) / K	ΔT(latt) / K	Structural data[a]
Group 1				
$[Fe(1\text{-}bpp)_2][BF_4]_2$	261[43]	248(1)[43]	13	HS/LS
$[Fe(bpp^{CH2OH,H})_2][BF_4]_2$	271[49]	229(2)[b]	42	HS/LS
$[Fe(bpp^{CH2OH,H})_2][ClO_4]_2$	284[50]	229(2)[b]	55	HS/LS
$[Fe(bpp^{Me,H})_2][ClO_4]_2$	184[44]	216(2)[17]	–32	HS
$[Fe(bpp^{F,H})_2][BF_4]_2$	237[17]	215(4)[17]	22	HS/LS
$[Fe(bpp^{H,Me})_2][ClO_4]_2$	233[50]	273(1)[17]	–40	HS/LS
$[Fe(bpp^{H,Cl})_2][BF_4]_2$	202[31]	231(3)[51]	–29	HS/LS
$[Fe(bpp^{H,Br})_2][BF_4]_2$	253[31]	238(2)[51]	15	HS
$[Fe(bpyz^{Me})_2][BF_4]_2$	242[52]	291(1)[52]	–49	HS
$[Fe(3\text{-}bpp)_2][NCS]_2$	230[26]	244(1)[27]	–12	HS/LS
$[Fe(3\text{-}bpp)_2][NCSe]_2$	234[25]	244(1)[27]	–10	HS
$[Fe(1,3\text{-}bpp)_2][ClO_4]_2$	315[53]	254[15,29]	61	LS
Group 2				
$[Fe(bpp^{SMe,H})_2][BF_4]_2$, mol A[c]	270[32]	194(2)[54]	76	HS/LS
$[Fe(bpp^{SMe,H})_2][BF_4]_2$, mol B[c]	269[32]	194(2)[54]	75	HS/LS
$[Fe(bpp^{SMe,H})_2][ClO_4]_2$, mol A[c]	253[54]	194(2)[54]	59	HS/LS
$[Fe(bpp^{SMe,H})_2][ClO_4]_2$, mol B[c]	258[54]	194(2)[54]	64	HS/LS
$[Fe(bpp^{Br,H})_2][BF_4]_2$	307[32]	234(1)[17]	73	HS/LS
$[Fe(bpp^{I,H})_2][BF_4]_2$	332[32]	236(1)[17]	96	HS/LS

$[Fe(bpp^{I,H})_2][ClO_4]_2$	333[55]	236(1)[17]	97	LS
$[Fe(bpp^{CH2Br,H})_2][BF_4]_2$	324[56]	237(10)[d]	87	LS
$[Fe(bpp^{CCH,H})_2][BF_4]_2$, phase A	341[38]	250(10)[d]	91	HS/LS
$[Fe(bpp^{CCH,H})_2][BF_4]_2$, phase B	440[37]	250(10)[d]	190	HS/LS
Group 3				
$[Fe(bpp^{SiPr,H})_2][BF_4]_2$	185[33]	215(4)[b]	–30	HS/LS
$[Fe(bpp^{SiPr,H})_2][BF_4]_2 \cdot MeNO_2$	171[33]	215(4)[b]	–44	HS/LS
$[Fe(bpp^{SiPr,H})_2][BF_4]_2 \cdot MeCN$	161[33]	215(4)[b]	–54	HS/LS
$[Fe(bpp^{SiPr,H})_2][BF_4]_2 \cdot yMe_2CO$	141[33]	215(4)[b]	–74	HS/LS
$[Fe(bpp^{SiPr,H})_2][BF_4]_2 \cdot H_2O$	212[33]	215(4)[b]	–3	HS/LS
$[Fe(bpp^{SiPr,H})_2][ClO_4]_2$	175[39]	215(4)[b]	–40	HS/LS
$[Fe(bpp^{SiPr,H})_2][ClO_4]_2 \cdot MeNO_2$	90[39]	215(4)[b]	–125	HS
$[Fe(bpp^{SiPr,H})_2][ClO_4]_2 \cdot H_2O$	176[39]	215(4)[b]	–39	HS/LS
Group 4				
$[Fe(1\text{-}bpp)_2][Ni(mnt)_2]_2 \cdot MeNO_2$	175[57,e]	248(1)[43]	–73	HS/LS
$[Fe(bpp^{CH2SCN,H})_2][BF_4]_2$	272[58]	213(1)[58]	59	HS/LS
$[Fe(bpp^{CO2H,H})_2][BF_4]_2$	347[59,60]	281(1)[17]	66	HS/LS
$[Fe(bpp^{CO2H,H})_2][ClO_4]_2$	383[60]	281(1)[17]	102	HS/LS
$[Fe(bpp^{CO2Et,H})_2][ClO_4]_2 \cdot MeCN$	233[45]	275(2)[61,f]	–42	HS
$[Fe(bpp^{C\{S\}NHMe,H})_2][ClO_4]_2$	332[62]	262(4)[62]	70	HS/LS
$[Fe(bpp^{CH=CHPh,H})_2][BF_4]_2 \cdot Me_2CO$	172[63]	151(10)[d]	21	HS/LS
$[Fe(bpp^{C6H4OH\text{-}4,H})_2][ClO_4]_2$	281[55]	218(10)[d]	63	LS
$[Fe(bpp^{C6H4CHO\text{-}4,H})_2][ClO_4]_2$	285[64]	225(10)[d]	60	LS
$[Fe(bpp^{3\text{-}Py,H})_2][BF_4]_2$	400[65]	245(10)[d]	155	LS
$[Fe(bpp^{3\text{-}Py,H})_2][ClO_4]_2$	406[65]	245(10)[d]	161	LS

$[Fe(bpyz)_2][BF_4]_2 \cdot 3MeNO_2$	198[66]	268(1)[52]	–70	HS/LS
$[Fe(3\text{-}bpp)_2][Fe(NO)(CN)_5]_2$	183[67]	244(1)[27]	–61	HS/LS

[a]HS, LS = high-spin or low-spin crystal structure available. HS/LS = structures in both spin states available. [b]This work (Figure S2). [c]Material contains two unique cations, which undergo SCO at discrete temperatures. [d]Estimated from our previously reported correlation for $T_{½}$(solution) in $[Fe(1\text{-}bpp)_2]^{2+}$ derivatives.[17] [e]This is the high-spin→low-spin $T_{½}$ in cooling mode. [f]Solution $T_{½}$ is for $[Fe(bpp^{CO2C16H33,H})_2][ClO_4]_2$.

An initial survey of the relationship between $T_{½}$(solid) or ΔT(latt) and molecular structure, for all the compounds in the Table, found no clear correlations. Therefore, the compounds were divided into groups, reflecting the crystal packing they adopt (Table 1). Group 1 all crystallize in variants of the "terpyridine embrace" lattice type, involving four-fold layers of interdigitated cations associating through $\pi\ldots\pi$ interactions between their pyrazolyl arms (Figure 1, top).[30] SCO iron(II) complexes adopting this lattice type often exhibit rather similar, abrupt spin transitions with narrow thermal hysteresis loops.[31] Group 2 all adopt a second crystal packing motif related to the terpyridine embrace, but with half the $\pi\ldots\pi$ contacts disrupted by the pyridyl ring 'X' substituents from adjacent cation layers (Chart 1; Figure 1, bottom).[32] Group 3 is a family of isostructural solvate crystals of the same complex cation, which adopt a third mode of crystal packing.[33] While group 3 is also a layered structure, cations within the layers are not all co-aligned, and are well-separated by *iso*propyl substituents and anions (Figure 2). Despite their structural similarities, compounds in groups 2 and 3 exhibit more varied SCO behavior than those in group 1. Lastly, group 4 contains other, structurally diverse compounds that do not fall

into the other groups. Groups 1, 2 and 4 all include some compounds undergoing crystallographic phase changes during SCO, and others that do not. Similarly, all the groups include materials with gradual, abrupt or hysteretic SCO transitions.

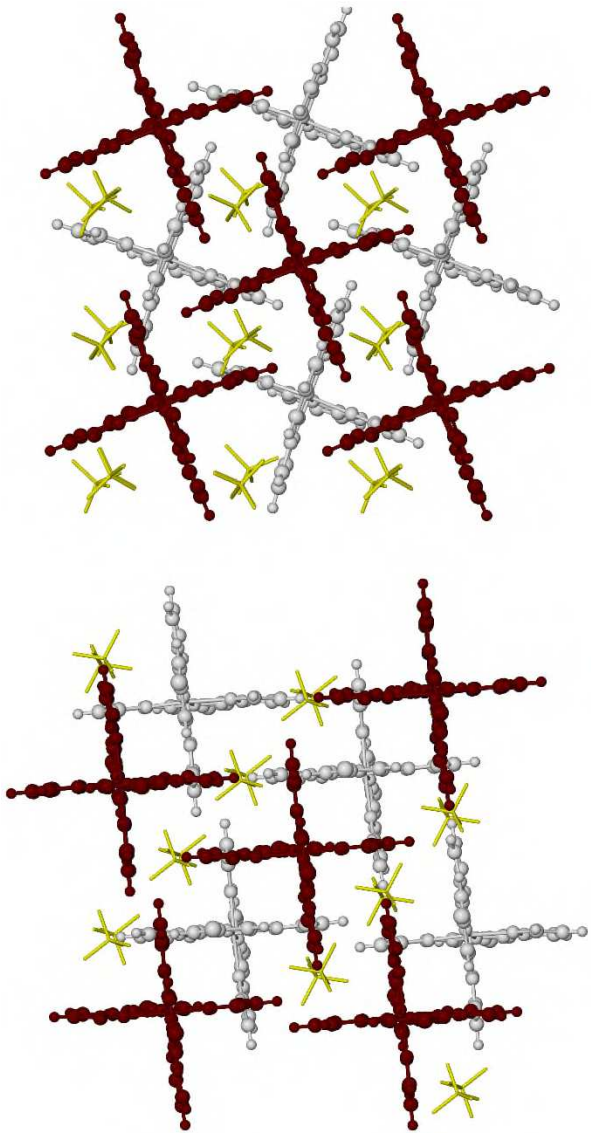

Figure 1 The crystal packing in representative examples of group 1 ($[Fe(1\text{-}bpp)_2][BF_4]_2$, top)[43] and group 2 ($[Fe(bpp^{Br,H})_2][BF_4]_2$, bottom),[32] oriented to highlight their similarities and differences. Alternate cation layers in these lattices have white and maroon coloration, while the BF_4^- ions are yellow. Different variants of the terpyridine lattice in group 1 have adjacent cation layers that are canted with respect to each other (as in the Figure), or are co-aligned.[30]

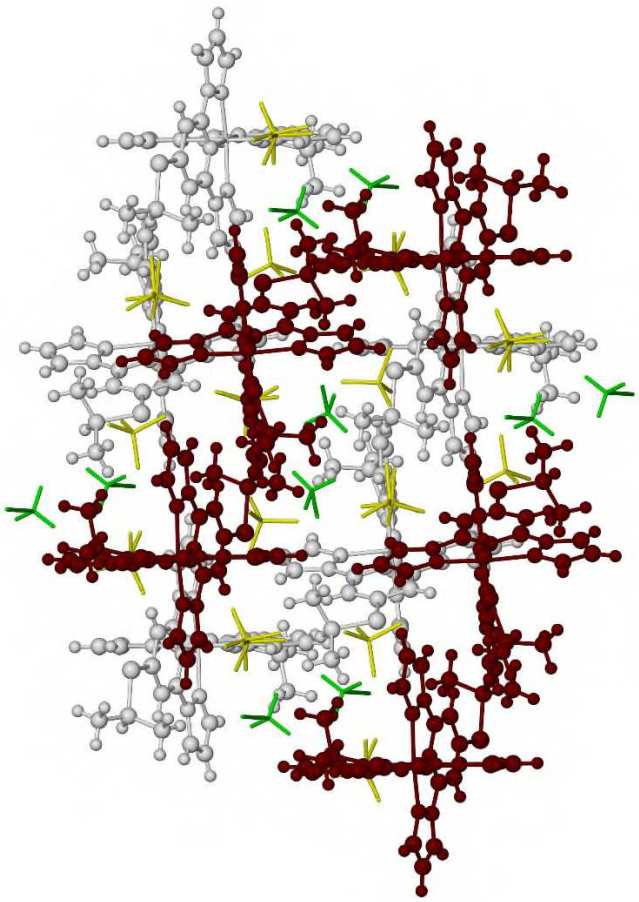

Figure 2 The crystal packing in a group 3 compound ($[Fe(bpp^{SiPr,H})_2][BF_4]_2 \cdot MeCN$),[33] oriented to highlight the difference with groups 1 and 2 (Figure 1). Alternate cation layers in the (100) plane have white and maroon coloration, the BF_4^- ions are yellow and MeCN molecules are green.

The ΔT(latt) values in the Table show some clear trends. Group 2 shows consistently large and positive ΔT(latt) which, with one exception, spans a small range of values ($59 \leq \Delta T(\text{latt}) \leq 91$ K). Thus that lattice type consistently stabilizes the low-spin form of a complex, to a similar extent in each of these cases. In contrast, ΔT(latt) for group 3 spans a wider range of negative values, implying that structure type stabilizes the high-spin state to varying degrees. Lastly, group 1

shows a range of positive and negative ΔT(latt) values, implying the terpyridine embrace lattice type has a significant, but inconsistent, influence on the spin state of those complexes.

$T_{½}$(solid) and ΔT(latt) for groups 1-3 were plotted against different metrics measuring changes in the metal coordination sphere (Figure 3). The compounds in each group are considered separately. The trends described below are followed by the majority of compounds. However, a few examples have different or unusual structural chemistry which makes them outliers in some, or all, of the correlations considered. These are discussed further below, and are highlighted in italics in Table 1 and with pale coloration in Figure 3.

The simplest parameter considered is V_{Oh}, the volume of the FeN_6 octahedron as a measure of the Fe–N bond distances.[34] V_{Oh} is typically <10 Å^3 in low-spin $[Fe(1\text{-bpp})_2]^{2+}$ derivatives, and ≥12 Å^3 in SCO-active high-spin compounds.[35] The change in V_{Oh} between the spin states is defined as ΔV_{Oh}, according to eq 2:

$$\Delta V_{Oh} = V_{Oh}(\text{high-spin}) - V_{Oh}(\text{low-spin}) \quad (2)$$

Alternative structural indices used to quantify the spin states of SCO compounds are the angular distortion parameters Σ and Θ (eqs 3 and 4):

$$\Sigma = \sum_{i=1}^{12} |90 - \beta_i| \quad (3)$$

$$\Theta = \sum_{j=1}^{24} |60 - \gamma_j| \quad (4)$$

where β_i are the twelve *cis*-N–Fe–N angles about the iron atom and γ_j are the 24 unique N–Fe–N angles measured on the projection of two triangular faces of the octahedron along their common pseudo-threefold axis (Chart 2). Σ is a general measure of the deviation of a metal ion from an ideal octahedral geometry, while Θ more specifically indicates its distortion towards a trigonal prismatic structure.[34,36] A perfectly octahedral complex gives $\Sigma = \Theta = 0$ (Guionneau *et al* used Θ in their study[12]). Σ and Θ are usually much larger in the high-spin state, particularly in complexes

of chelating ligands with restricted bite angles as in this work.[10] Hence, changes in Σ and Θ between the spin states ($\Delta\Sigma$ and $\Delta\Theta$) reflect the angular rearrangement of the coordination sphere during SCO.

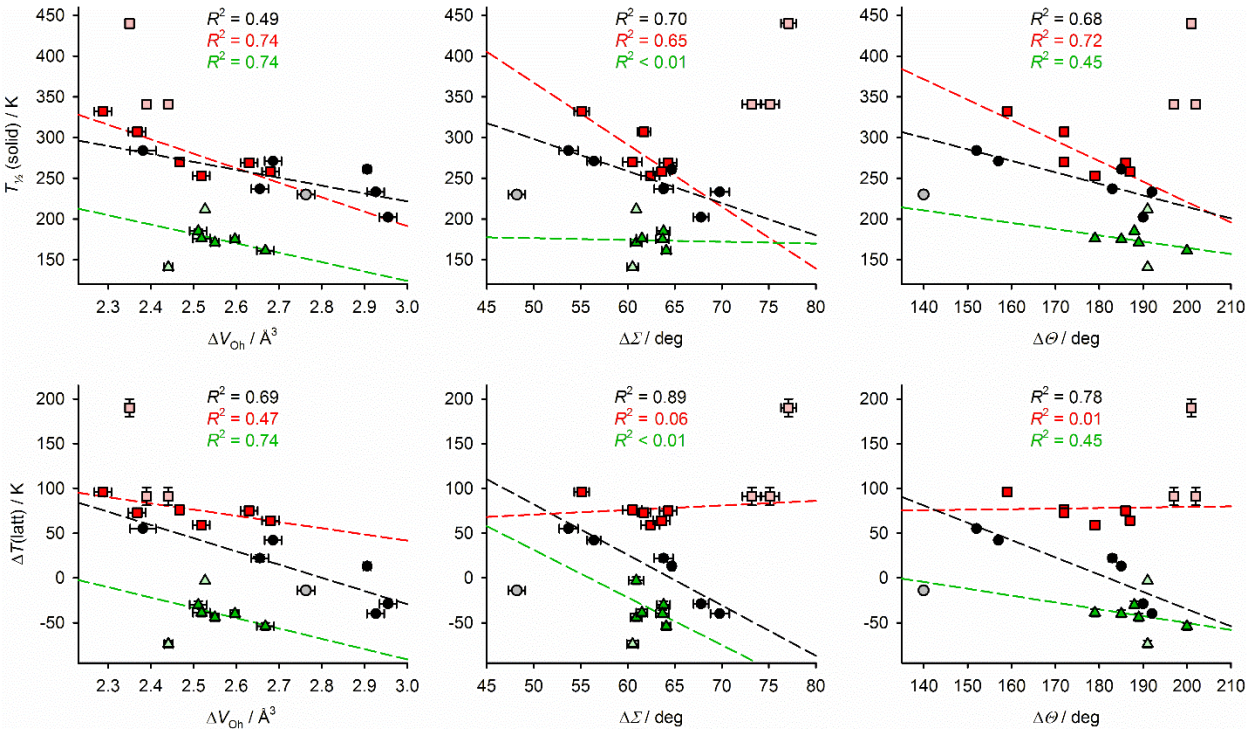

Figure 3 The relationship between $T_{½}$(solid) (top) and ΔT(latt) (bottom) and three indices describing changes to the metal ion coordination sphere during SCO. Error bars are often smaller than the symbols on the graphs. The compounds are plotted as group 1 (black or gray circles), group 2 (dark or pale red squares) and group 3 (dark or pale green triangles). The dotted lines show the linear regression lines for each group of compounds, excluding the outlier compounds shown in pale coloration. Correlation coefficients for these regression lines are shown for each graph. Near-zero correlation coefficients imply the data are highly scattered, and/or that the slope of the regression line is near zero so the plotted parameters have no influence on each other.

Chart 2. Angles used in the definitions of the distortion parameters Σ and Θ.

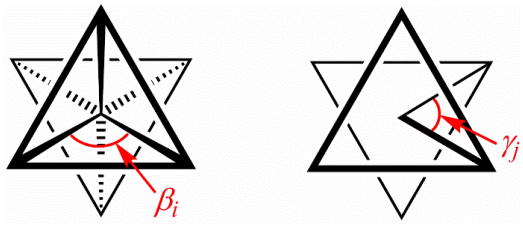

The three groups of compounds in Table 1 exhibit markedly different behaviors against these structural parameters. The $[Fe(1\text{-bpp})_2]^{2+}$ complexes in group 1 (black circles) show consistent negative correlations of ΔV_{Oh}, $\Delta\Sigma$ and $\Delta\Theta$ against both $T_{½}$(solid) and ΔT(latt), although the fits to ΔT(latt) have consistently better linearity (higher regression R^2 values) than the corresponding $T_{½}$(solid) plots. The one $[Fe(3\text{-bpp})_2]^{2+}$ complex of this type where structural data are available in both spin states (gray circle) matches the rest of the group in its ΔV_{Oh} bond length parameter, but is a strong outlier in the angular $\Delta\Sigma$ and $\Delta\Theta$ plots. We attribute that to the different bite angle exerted by 3-bpp, whose heterocyclic rings are linked by C–C bonds, compared to the slightly shorter C–N bonds linking the donor groups in 1-bpp or bpyz. This is reflected in tabulated Σ and Θ values for $[Fe(1\text{-bpp})_2]^{2+}$ and $[Fe(3\text{-bpp})_2]^{2+}$ derivatives which are, on average, *ca* 10 % lower for $[Fe(1\text{-bpp})_2]^{2+}$ in its low-spin form, and *ca* 5 % higher in the high-spin state.[37] Hence, although their bond length properties (V_{Oh}) are similar, $[Fe(3\text{-bpp})_2]^{2+}$ complexes generally exhibit $\Delta\Sigma$ and $\Delta\Theta$ values that are *ca* 25 % smaller than for $[Fe(1\text{-bpp})_2]^{2+}$ derivatives, all other things being equal. That is consistent with our observations (Figure 3).

$T_{½}$(solid) shows a reasonable correlation with these structural indices for most of group 2 (Figure 3, red squares), but with two strong outlier materials. These are two low-spin phases of the same complex which, unusually, interconvert upon cycling about the spin transition *via* the

same high-spin phase.[38] In contrast, the structural dependency of ΔT(latt) for group 2 is much weaker, showing a shallow negative correlation with ΔV_{Oh} and essentially zero correlation with the angular parameters. However, those weaker correlations also now account for one of the outlier materials, which is not described by the $T_{½}$(solid) analyses. Hence, the ΔT(latt) parameter gives a more consistent description of this group, in which the lattice imposes an almost constant additional stabilization of the low-spin state. Thus, $T_{½}$(solid) in group 2 is less influenced by molecular structure changes during SCO than in group 1.

The group 3 materials (Figure 3, green triangles) all contain the same complex cation, giving the same $T_{½}$(solution) correction in their ΔT(latt) values (Table 1). Hence, the $T_{½}$(solid) and ΔT(latt) correlations are identical for this group. Five of these compounds show a good linear relationships between ΔT(latt) and ΔV_{Oh} or $\Delta\Theta$, although the latter correlation is very shallow. There are two significant outliers in the group, however, for reasons that are unclear. It is suggestive that the outliers have the highest and lowest $T_{½}$(solid) and ΔT(latt) values in the group, but there are no structural aspects unique to those compounds to explain their apparently anomalous properties (but see below).[33,39] The $\Delta\Sigma$ values in this group span a narrow range, and there is no apparent correlation of that parameter with ΔT(latt).

Equivalent plots of $T_{½}$(solid) and ΔT(latt) *vs* V_{Oh}, Σ or Θ in the high-spin (HS) or low-spin (LS) states of the compounds were also examined, to investigate whether either spin state makes a dominant contribution to the above trends (Figure 4). These graphs also included some extra compounds, whose crystal structures are only available in one spin state (Table 1). Groups 1-3 again show different behavior in these plots.

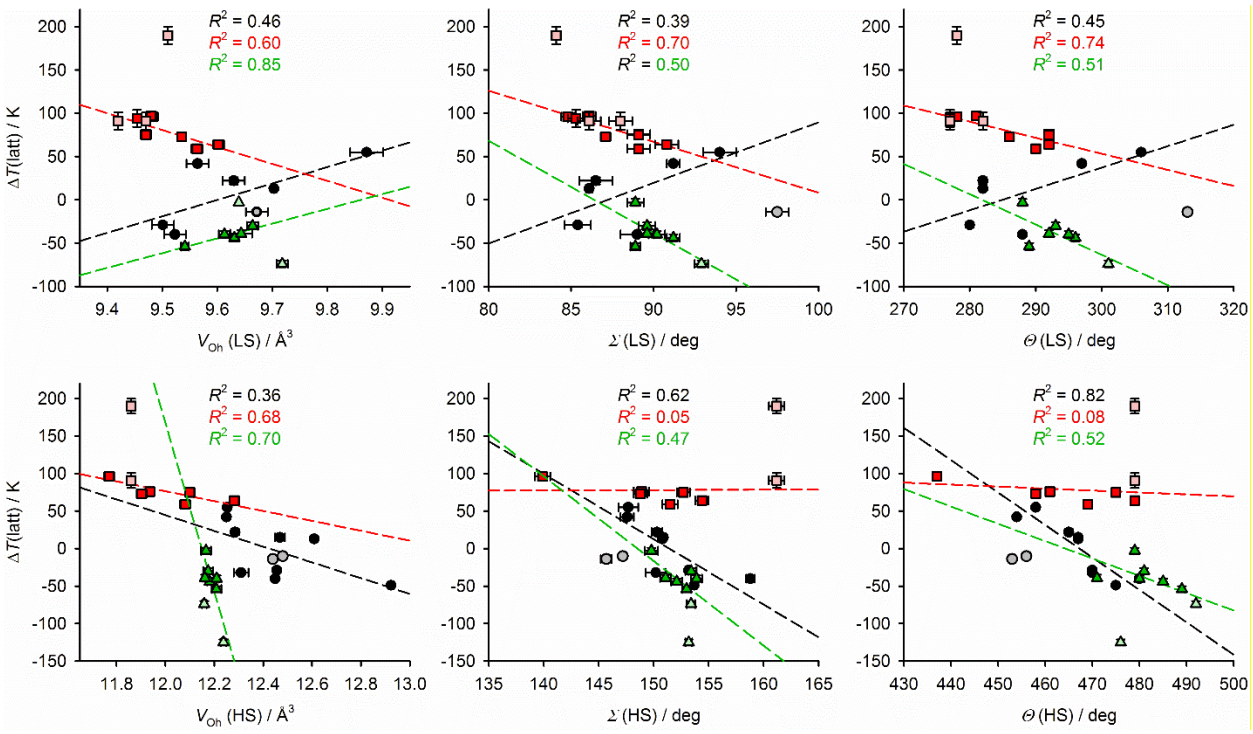

Figure 4 The relationship between ΔT(latt) and three indices describing the metal ion coordination sphere during SCO, in the low-spin (LS, top) and high-spin (HS, bottom) compounds. Details as for Figure 3.

While the data are more scattered than in Figure 3, group 1 shows moderately linear positive correlations between V_{Oh}(LS), Σ(LS) or Θ(LS) and ΔT(latt), and comparable negative correlations between ΔT(latt) and the same parameters in the HS state (Figure 4). There is no consistent trend in the slope of those correlations between the spin states, so neither spin state clearly dominates the behavior of group 1. However, the apparent stabilization of the low-spin state by expansion of the metal coordination sphere in the LS correlations is counter-intuitive. We interpret that as confirming that the *change* in these parameters during SCO is the important factor controlling ΔT(latt) in the group 1 compounds (Figure 3).

The plots of ΔT(latt) *vs* V_{Oh}, Σ or Θ in each spin state of group 2 have good linearity, which includes one of the group outliers as above (Figure 4). The LS parameters all show negative correlations with ΔT(latt) with more negative slopes than the equivalent HS regression lines, some of which have essentially zero slope. Hence, the LS state evidently contributes more to the relationship between ΔT(latt) and ΔV_{Oh} for this group (Figure 3).

In group 3, a positive correlation between ΔT(latt) and V_{Oh}(LS) is counterbalanced by a much steeper negative linear correlation to V_{Oh}(HS) (Figure 4). The latter is the only structure:function relationship we have identified which accounts for all the outlier compounds in group 3. We therefore suggest the Fe–N bond lengths in the high-spin state are the biggest contributor to ΔT(latt) and $T_{½}$(solid) in group 3. Consistent with that, another member of that series which remains fully high-spin on cooling, $[Fe(bpp^{SiPr,H})_2][ClO_4]_2 \cdot MeCN$, exhibits a larger V_{Oh}(HS) value of 12.254(7) Å^3 at 142 K.[39] That gives a predicted ΔT(latt) = –147 K, or $T_{½}$(solid) = 68 K, from the correlation in Figure 4. SCO in $[Fe(1\text{-bpp})_2]^{2+}$ and $[Fe(3\text{-bpp})_2]^{2+}$ derivatives rarely extends below 100 K,[39-41] where they become kinetically trapped in their high spin states.[39,40,42] Correlations between ΔT(latt) and Σ or Θ for group 3 in each spin state are all negative, and more scattered than the V_{Oh} plots.

All the corresponding graphs for group 4 are very scattered and contain no identifiable structure:function correlations (Figures S3 and S4). That is consistent with our other results, implying that crystal packing plays an important role in the relationship between structure and SCO in these compounds.

Two more structural indices that are often applied to $[Fe(1\text{-bpp})_2]^{2+}$ or $[Fe(3\text{-bpp})_2]^{2+}$ derivatives are ϕ (the *trans*-N{pyridyl}–Fe–N{pyridyl} angle) and θ (the dihedral angle between the least squares planes of the two ligands; Chart 3).[43] ϕ and θ reflect the relative disposition of

the two ligands in the complex, and thus describe the shape of the molecule as a whole rather than simply the inner coordination sphere. Significant changes in ϕ and θ during SCO can be associated with enhanced cooperativity in the transitions.[44,45] However, larger deviations of ϕ and θ from their ideal values of $\phi = 180°$ and $\theta = 90°$, tend to inhibit SCO in the solid state.[14,15,46] Since ϕ and θ are influenced by intermolecular interactions as well as the metal coordination geometry, they can deviate from ideality in both spin states. Hence, $\Delta\phi$ and $\Delta\theta$ (defined as in eq 2) can take positive or negative values.

Chart 3 The distortion parameters ϕ and θ in $[Fe(1\text{-bpp})_2]^{2+}$ derivatives.

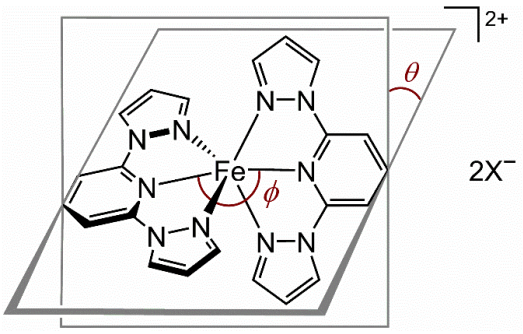

Linear relationships can be identified between ΔT(latt) and $\Delta\theta$ for groups 1 and 3. For group 1, a negative correlation between these parameters includes the outlier $[Fe(3\text{-bpp})_2][NCS]_2$ (Table 1), but excludes two other compounds in the series (Figure 5, top). That implies larger distortions along the θ coordinate in the high-spin state tend to stabilize the high-spin form of the complexes, which is reasonable. However, $\Delta\theta$ and ΔV_{Oh} also correlate well for most of this group (Figure 5, bottom) while there are also weaker correlations between $\Delta\theta$, and $\Delta\Sigma$ or $\Delta\Theta$, for the same compounds (Figure S7). Hence, the molecular shape and inner coordination sphere are

interrelated in this group, and no one structural parameter can be identified as the main contributor to their ΔT(latt).

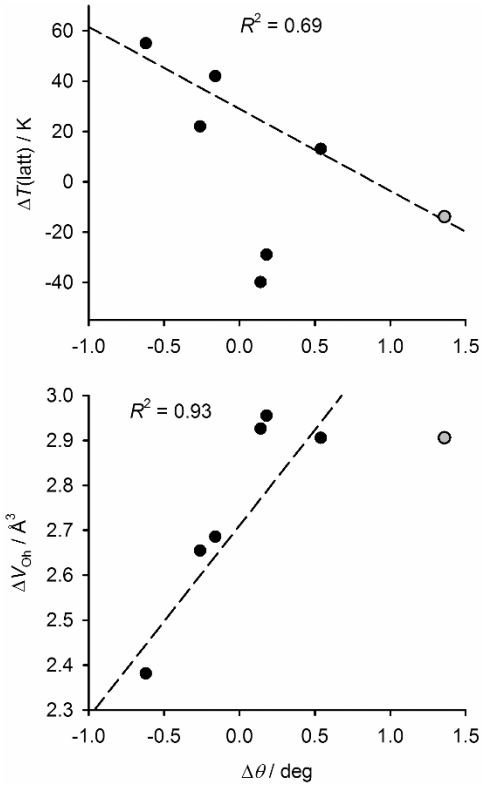

Figure 5 Top: the relationship between ΔT(latt) and $\Delta\theta$ for group 1, showing a correlation involving a subset of the group. Bottom: plot of ΔV_{Oh} *vs* $\Delta\theta$ for the same compounds, showing a link between their molecular shape and the dimensions of their inner coordination sphere. The gray point is the outlier compound for the group in Figures 3 and 4 (Table 1).

Moderately linear correlations between ΔT(latt) and $\Delta\phi$ or $\Delta\theta$ can be proposed for group 3 (Figure S6), excluding the outlier compounds in Table 1 which is consistent with Figures 1 and 2. These are mirrored in plots of ΔT(latt) *vs* ϕ or θ in the high-spin state of the materials, which supports the validity of that relationship (Figure S8). However, an alternative linear relationship is also apparent between ΔT(latt) and $\Delta\theta$ only, for five of the seven compounds including the

outliers but excluding two other compounds in the group (Figure S6). In contrast to group 1, there is no clear link between $\Delta\theta$ and V_{Oh}, Σ or Θ for this group (Figure S8) so the interpretation of this observation is less clear.

There is no correlation between ΔT(latt) and $\Delta\phi$ or $\Delta\theta$ for the group 2 and group 4 compounds (Figures S4 and S6). Moreover, these geometric distortions cannot explain the outlier compounds in groups 1-3, since none of these has unusually large $\Delta\phi$ or $\Delta\theta$ values compared to the other compounds (Table S2).

Conclusion

We have used the available library of $[Fe(1\text{-bpp})_2]^{2+}$ derivatives, and a handful of related compounds, to reproduce Guionneau *et al*'s observation that $T_{½}$ in solid SCO complexes correlates with common measures of the rearrangement of the metal coordination sphere during SCO (Figure S1).[12,34] Larger structural changes about the iron center generally stabilize the high-spin form of the compound, thus increasing $T_{½}$. In this study, though, that relationship is only evident among isostructural or near-isostructural materials, which adopt the same mode of crystal packing. The degree to which structure influences $T_{½}$ varies between these different lattice types. However, the correlations mostly hold equally well for materials exhibiting phase changes or thermal hysteresis during SCO, as for those that do not (although a compound in group 2 is a consistent exception). It is also equally valid for compounds undergoing SCO above or below room temperature. Notably, most of the crystals in Guionneau's correlation are also closely related, in adopting one of three variants of the same packing mode.[12,13,47]

The parameter ΔT(latt) provides insight into these differences, by separating out the contributions to $T_{½}$(solid) from the metal ion ligand field, and from the surrounding lattice. In the group 1 compounds (Table 1), both these elements contribute to $T_{½}$(solid), and ΔT(latt) correlates well with several measures of the molecular changes occurring during SCO. However, small differences in ligand bite angle between the isomeric members of the $[Fe(bpp)_2]^{2+}$ family (Chart 1) change their Σ and Θ values sufficiently, that only the bond length parameter ΔV_{Oh} describes all the compounds in the group consistently.

In contrast, while the compounds in group 2 exhibit comparable ΔV_{Oh}, $\Delta\Sigma$ and $\Delta\Theta$ values to group 1, these have a much weaker influence on ΔT(latt) which mostly spans a small range of positive values. Hence, that lattice type is insensitive to molecular structure changes during SCO, but exerts a more consistent stabilization of the low-spin state across the whole group of materials. Consistent with that, the low-spin structures of those compounds appear to contribute more than the high-spin to ΔT(latt) in those compounds (Figure 4). One outlier material in group 2 is a consistent exception to that trend; that compound exhibits an unusual phase change during SCO, whose energetics could also contribute to ΔT(latt) in that case.[38] However, in other respects group 2 is the most predictable series of compounds in this work, since their $T_{½}$(solid) temperatures are most closely related to the electronic properties of the ligands in the compound. Thus, eq 5 predicts $T_{½}$(solid) for all the group 2 compounds, excluding the outlier, to within ±20 K based on the σ_p^+ Hammett parameters of their ligand substituents (Table 2).[48]

$$T_{½}(\text{solid}) = 80\sigma_p^+ + 310 \qquad (5)$$

The group 2 compounds all have some chemical similarity, in containing pyridyl ligand substituents with one or two heavy atoms and no substituents at the pyrazolyl rings. While not all

such compounds lie in group 2 (Table 1), other complexes with that substituent pattern are most likely to adopt the group 2 crystal packing, and to show the predictable behavior of eq 5.

Table 2. $T_{½}$(solid) values calculated by eq 5 for the group 2 compounds (Table 1), based on the σ_p^+ Hammett parameters of their pyridyl ligand substituents.[48] The outlier phase B of $[Fe(bpp^{CCH,H})_2][BF_4]_2$ is omitted from the list.

	σ_p^+	$T_{½}$(solid) obsd / K	$T_{½}$(solid) calcd / K
$[Fe(bpp^{SMe,H})_2][BF_4]_2$, mol A[32]	−0.60	270	262
$[Fe(bpp^{SMe,H})_2][BF_4]_2$, mol B[32]	−0.60	269	262
$[Fe(bpp^{SMe,H})_2][ClO_4]_2$, mol A[54]	−0.60	253	262
$[Fe(bpp^{SMe,H})_2][ClO_4]_2$, mol B[54]	−0.60	258	262
$[Fe(bpp^{Br,H})_2][BF_4]_2$[32]	0.15	307	322
$[Fe(bpp^{I,H})_2][BF_4]_2$[32]	0.14	332	321
$[Fe(bpp^{I,H})_2][ClO_4]_2$[55]	0.14	333	321
$[Fe(bpp^{CH2Br,H})_2][BF_4]_2$[56]	0.02	324	312
$[Fe(bpp^{CCH,H})_2][BF_4]_2$, phase A[38]	0.18	341	324

The behavior of group 3 is harder to rationalize, despite this being the most similar group of materials in Table 1. Unlike group 2, all the variation in $T_{½}$(solid) for this group comes from the ΔT(latt) lattice contribution. So, no correlation equivalent to eq 5 can be written for group 3. Although all members of group 3 are perfectly isostructural in both spin states, three of its eight compounds are outliers behaving differently from the others in most of the correlations examined. Unlike the group 2 outlier, there is no exceptional phase behavior in those compounds

to rationalize that variation. Only one parameter was found that fits ΔT(latt) for all members of the group, through a very steep correlation with the Fe–N bond lengths (V_{Oh}) in the high-spin compounds. Hence, in contrast to group 2, the high-spin structures of group 3 may control the lattice contribution to their $T_{½}$(solid) values. That is consistent with ΔT(latt) for this group, whose lattice stabilizes the high-spin form of all the compounds to varying degrees (Table 1).

In all three of these groups, ΔT(latt) is better described by measures of the inner metal coordination sphere (V_{Oh}, Σ and Θ), than by parameters describing the shape of the molecule as a whole (θ and ϕ). That implies different considerations may apply to the temperature and cooperativity of SCO in a solid material. Anisotropic crystal packing and short intermolecular contacts that deform the shape of a molecule often lead to more cooperative spin transitions.[10,13] However, taken together, this work and ref 12 imply crystal packing might only influence $T_{½}$ significantly, if that lattice anisotropy results in a distortion of the inner coordination sphere.

In conclusion, we have introduced the ΔT(latt) parameter as a useful aid to understanding the molecular and lattice contributions to $T_{½}$(solid) in molecular SCO crystals. Different crystal lattices in this study influence $T_{½}$(solid) consistently, but in different ways. For example, ΔT(latt) in a lattice that consistently stabilizes the low-spin state of a molecule is more strongly influenced by its low-spin molecular structure, and *vice versa*. That observation may have predictive value for the crystal engineering of SCO molecular materials, and deserves further investigation.

ASSOCIATED CONTENT

Supporting Information The following material is available free of charge via the Internet at http://pubs.acs.org.

Previously unpublished solution-phase magnetic susceptibility data; the tabulated structural parameters discussed in the text; additional structure:function plots; and crystallographic and magnetic susceptibility data from the new anhydrous phase of $[Fe(3\text{-bpp})_2][NCS]_2$.

X-ray crystal structures of $[Fe(3\text{-bpp})_2][NCS]_2$: CCDC 1903939-1903941 (CIF).

AUTHOR INFORMATION

Corresponding Author

*Email: m.a.halcrow@leeds.ac.uk

ORCID

Malcolm A. Halcrow: 0000-0001-7491-9034

Izar Capel Berdiell: 0000-0003-3828-7097

Christopher M. Pask: 0000-0002-2241-5069

Rafal Kulmaczewski: 0000-0002-3855-4530

Notes

The authors declare no competing financial interest. Experimental data sets associated with this paper are available from the University of Leeds library (http://doi.org/10.5518/###)

ACKNOWLEDGEMENTS

This work was funded by the Leverhulme Trust (RPG-2015-095), the EPSRC (EP/K012576/1) and the University of Leeds. The authors thank Oscar Cespedes (School of Physics and Astronomy, University of Leeds) and Mark Howard (School of Chemistry, University of Leeds) for help with the solid state and solution-phase magnetic measurements in the Supporting Information.

REFERENCES

(1) (a) *Spin Crossover in Transition Metal Compounds I−III, Topics in Current Chemistry*; Gütlich, P., Goodwin, H. A., Eds.; Springer-Verlag: Berlin, 2004; Vols. 233−235. (b) Halcrow, M. A. (ed), *Spin-Crossover Materials - Properties and Applications,* John Wiley & Sons, Ltd.: New York, 2013, p. 568.

(2) (a) Kumar, K. S.; Ruben, M. Emerging Trends in Spin Crossover (SCO) Based Functional Materials and Devices. *Coord. Chem. Rev.* **2017**, *346*, 176–205. (b) Molnár, G.; Rat, S.; Salmon, L.; Nicolazzi, W.; Bousseksou, A. Spin Crossover Nanomaterials: From Fundamental Concepts to Devices. *Adv. Mater.* **2018**, *30*, 17003862/1–23. (c) Zarembowitch, J.; Varret, F.; Hauser, A.; Real, J. A.; Boukheddaden, K. Spin Crossover Phenomenon – Preface and Introduction *C. R. Chimie* **2018**, *21*, 1056–1059.

(3) See eg (a) Takahashi, K.; Cui, H.-B.; Okano, Y.; Kobayashi, H.; Mori, H.; Tajima, H.; Einaga, Y; Sato, O. Evidence of the Chemical Uniaxial Strain Effect on Electrical Conductivity

in the Spin-Crossover Conducting Molecular System: $[Fe^{III}(qnal)_2][Pd(dmit)_2]_5 \cdot$acetone. *J. Am. Chem. Soc.* **2008**, *130*, 6688–6689. (b) Rotaru, A.; Gural'skiy, I. A.; Molnár, G.; Salmon, L.; Demont, P.; Bousseksou, A. Spin State Dependence of Electrical Conductivity of Spin Crossover Materials. *Chem. Commun.* **2012**, *48*, 4163–4165. (c) Phan, H.; Benjamin, S. M.; Steven, E.; Brooks, J. S.; Shatruk, M. Photomagnetic Response in Highly Conductive Iron(II) Spin-Crossover Complexes with TCNQ Radicals. *Angew. Chem. Int. Ed.* **2015**, *54*, 823–827. (d) Wang, H.-Y.; Ge, J.-Y.; Hua, C.; Jiao, C.-Q.; Wu, Y.; Leong, C. F.; D'Alessandro, D. M.; Liu, T.; Zuo, J.-L. Photo- and Electronically Switchable Spin-Crossover Iron(II) Metal-Organic Frameworks Based on a Tetrathiafulvalene Ligand. *Angew. Chem. Int. Ed.* **2017**, *56*, 5465–5470.

(4) See *eg* (a) Bonhommeau, S.; Guillon, T.; Daku, L. M. L.; Demont, P.; Costa, J. S.; Létard, J.-F.; Molnár, G.; Bousseksou, A. Photoswitching of the Dielectric Constant of the Spin-Crossover Complex $[Fe(L)(CN)_2]\cdot H_2O$. *Angew. Chem. Int. Ed.* **2006**, *45*, 1625–1629. (b) Zhang, X.; Mu, S.; Chastanet, G.; Daro, N.; Palamarciuc, T.; Rosa, P.; Létard, J.-F.; Liu, J.; Sterbinsky, G. E.; Arena, D. A.; Etrillard, C.; Kundys, B.; Doudin, B.; Dowben, P. A. Complexities in the Molecular Spin Crossover Transition. *J. Phys. Chem. C* **2015**, *119*, 16293–16302. (c) Bovo, G.; Bräunlich, I.; Caseri, W. R.; Stingelin, N.; Anthopoulos, T. D.; Sandeman, K. G.; Bradley, D. D. C.; Stavrinou, P. N. Room Temperature Dielectric Bistability in Solution-Processed Spin Crossover Polymer Thin Films. *J. Mater. Chem. C* **2016**, *4*, 6240–6248. (d) Diaconu, A.; Lupu, S.-L.; Rusu, I.; Risca, I.-M.; Salmon, L.; Molnár, G.; Bousseksou, A.; Demont, P.; Rotaru, A. Piezoresistive Effect in the $[Fe(Htrz)_2(trz)](BF_4)$ Spin Crossover Complex. *J. Phys. Chem. Lett.* **2017**, *8*, 3147–3151.

(5) Manrique-Juárez, M. D.; Rat, S.; Salmon, L.; Molnár, G.; Quintero, C. M.; Nicu, L.; Shepherd, H. J.; Bousseksou, A. Switchable Molecule-Based Materials for Micro- and Nanoscale Actuating Applications: Achievements and Prospects. *Coord. Chem. Rev.* **2016**, *308*, 395–408.

(6) See eg (a) Edder, C.; Piguet, C.; Bünzli, J.-C. G.; Hopfgartner, G. High- Spin Iron(II) as a Semitransparent Partner for Tuning Europium(III) Luminescence in Heterodimetallic d–f Complexes. *Chem. Eur. J.* **2001**, *7*, 3014–3024. (b) Garcia, Y.; Robert, F.; Naik, A. D.; Zhou, G.; Tinant, B.; Robeyns, K.; Michotte, S.; Piraux, L. Spin Transition Charted in a Fluorophore-Tagged Thermochromic Dinuclear Iron(II) Complex. *J. Am. Chem. Soc.* **2011**, *133*, 15850–15853. (c) Wang, C.-F.; Li, R.-F.; Chen, X.-Y.; Wei, R.-J.; Zheng, L.-S.; Tao, J. Synergetic Spin Crossover and Fluorescence in One-Dimensional Hybrid Complexes. *Angew. Chem. Int. Ed.* **2015**, *54*, 1574–1577. (d) Santoro, A.; Kershaw Cook, L. J.; Kulmaczewski, R.; Barrett, S. A.; Cespedes, O.; Halcrow, M. A. Iron(II) Complexes of Tridentate Indazolylpyridine Ligands: Enhanced Spin-Crossover Hysteresis, and Ligand-Based Fluorescence. *Inorg. Chem.* **2015**, *54*, 682–693. (e) Suleimanov, I.; Kraieva, O.; Costa, J. S.; Fritsky, I. O.; Molnár, G.; Salmon, L.; Bousseksou, A. Electronic Communication Between Fluorescent Pyrene Excimers and Spin Crossover Complexes in Nanocomposite Particles. *J. Mater. Chem. C* **2015**, *3*, 5026–5032. (f) Herrera, J. M.; Titos-Padilla, S.; Pope, S. J. A.; Berlanga, I.; Zamora, F.; Delgado, J. J.; Kamenev, K. V.; Wang, X.; Prescimone, A.; Brechin, E. K.; Colacio, E. Studies on Bifunctional Fe(II)-Triazole Spin Crossover Nanoparticles: Time-Dependent Luminescence, Surface Grafting and the Effect of a Silica Shell and Hydrostatic Pressure on the Magnetic Properties. *J. Mater. Chem. C* **2015**, *3*, 7819–7829. (g) Lochenie, C.; Schötz, K.; Panzer, F.; Kurz, H.; Maier, B.; Puchtler, F.; Agarwal, S.; Köhler, A.; Weber, B. Spin-Crossover Iron(II) Coordination Polymer with Fluorescent Properties: Correlation between Emission Properties and Spin State. *J. Am.*

Chem. Soc. **2018**, *140*, 700−709. (h) Wang, J.-L.; Liu, Q.; Meng, Y.-S.; Liu, X.; Zheng, H.; Shi, Q.; Duan, C.-Y.; Liu, T. Fluorescence Modulation via Photoinduced Spin Crossover Switched Energy Transfer from Fluorophores to Fe^{II} Ions. *Chem. Sci.* **2018**, *9*, 2892−2897. (i) Yuan, J.; Wu, S.-Q.; Liu, M.-J.; Sato, O.; Kou, H.-Z. Rhodamine 6G-Labeled Pyridyl Aroylhydrazone Fe(II) Complex Exhibiting Synergetic Spin Crossover and Fluorescence. *J. Am. Chem. Soc.* **2018**, *140*, 9426−9433.

(7) (a) Bonhommeau, S.; Lacroix, P. G.; Talaga, D.; Bousseksou, A.; Seredyuk, M.; Fritsky, I. O.; Rodriguez, V. Magnetism and Molecular Nonlinear Optical Second-Order Response Meet in a Spin Crossover Complex. *J. Phys. Chem. C* **2012**, *116*, 11251−11255. (b) Ohkoshi, S.; Takano, S.; Imoto, K.; Yoshikiyo, M.; Namai, A.; Tokoro, H. 90-Degree Optical Switching of Output Second-Harmonic Light in Chiral Photomagnet. *Nature Photon.* **2014**, *8*, 65−71.

(8) See *eg* (a) Ababei, R.; Pichon, C.; Roubeau, O.; Li, Y.-G.; Bréfuel, N.; Buisson, L.; Guionneau, P.; Mathonière, C.; Clérac, R. Rational Design of a Photomagnetic Chain: Bridging Single-Molecule Magnets with a Spin-Crossover Complex. *J. Am. Chem. Soc.* **2013**, *135*, 14840–14853. (b) Feng, X.; Mathonière, C.; Jeon, I.-R.; Rouzières, M.; Ozarowski, A.; Aubrey, M. L.; Gonzalez, M. I.; Clérac, R.; Long, J. R. Tristability in a Light-Actuated Single-Molecule Magnet. *J. Am. Chem. Soc.* **2013**, *135*, 15880–15884. (c) Mathonière, C.; Lin, H.-J.; Siretanu, D.; Clérac, R.; Smith, J. M. Photoinduced Single-Molecule Magnet Properties in a Four-Coordinate Iron(II) Spin Crossover Complex. *J. Am. Chem. Soc.* **2013**, *135*, 19083–19086. (d) Liu, T.; Zheng, H.; Kang, S.; Shiota, Y.; Hayami, S.; Mito, M.; Sato, O.; Yoshizawa, K.; Kanegawa, S.; Duan, C. Y. A Light-Induced Spin Crossover Actuated Single-Chain Magnet. *Nature Commun.* **2013**, *4*, 2826/1–7. (e) Shao, D.; Shi, L.; Yin, L.; Wang, B.-L.; Wang, Z.-X.; Zhang, Y.-Q.;

Wang, X.-Y. Reversible On-Off Switching of Both Spin Crossover and Single-Molecule Magnet Behaviours via a Crystal-To-Crystal Transformation. *Chem. Sci.* **2018**, *9*, 7986–7991.

(9) (a) Ohkoshi, S.; Imoto, K.; Tsunobuchi, Y.; Takano, S.; Tokoro, H. Light-Induced Spin-Crossover Magnet. *Nature Chem.* **2011**, *3*, 564−569; (b) Clemente-León, M.; Coronado, E.; López-Jordà, M.; Desplanches, C.; Asthana, S.; Wang, H.; Létard, J.-F. A Hybrid Magnet with Coexistence of Ferromagnetism and Photoinduced Fe(III) Spin-Crossover. *Chem. Sci.* **2011**, *2*, 1121–1127. (c) Rodríguez-Velamazán, J. A.; Fabelo, O.; Beavers, C. M.; Natividad, E.; Evangelisti, M.; Roubeau, O. A Multifunctional Magnetic Material Under Pressure. *Chem. Eur. J.* **2014**, *20*, 7956–7961. (d) Urtizberea, A.; Roubeau, O. Switchable Slow Relaxation of Magnetization in the Native Low Temperature Phase of a Cooperative Spin-Crossover Compound. *Chem. Sci.* **2017**, *8*, 2290–2295.

(10) Halcrow, M. A. Structure:Function Relationships in Molecular Spin-Crossover Complexes. *Chem. Soc. Rev.* **2011**, *40*, 4119−4142.

(11) (a) Bertoni, R.; Cammarata, M.; Lorenc, M.; Matar, S. F.; Létard, J.-F.; Lemke, H. T.; Collet, E. Ultrafast Light-Induced Spin-State Trapping Photophysics Investigated in $Fe(phen)_2(NCS)_2$ Spin-Crossover Crystal. *Acc. Chem. Res.* **2015**, *48*, 774–781. (b) Bertoni, R.; Lorenc, M.; Tissot, A.; Boillot, M.-L.; Collet, E. Femtosecond Photoswitching Dynamics and Microsecond Thermal Conversion Driven by Laser Heating in Fe^{III} Spin-Crossover Solids. *Coord. Chem. Rev.* **2015**, *282–283*, 66–76.

(12) Marchivie, M.; Guionneau, P.; Létard, J.-F.; Chasseau, D. Photo-Induced Spin-Transition: the Role of the Iron(II) Environment Distortion. *Acta Cryst. Sect. B Struct. Sci*. 2005, **61**, 25−28.

(13) Buron-Le Cointe, M.; Hébert, J.; Baldé, C.; Moisan, N.; Toupet, L.; Guionneau, P.; Létard, J.-F.; Freysz, E.; Cailleau, H.; Collet, E. Intermolecular Control of Thermoswitching and Photoswitching Phenomena in Two Spin-Crossover Polymorphs. *Phys. Rev. B* **2012**, *85*, 064114/1–9.

(14) Halcrow, M. A. Iron(II) Complexes of 2,6-Di(pyrazol-1-yl)pyridines – a Versatile System for Spin-Crossover Research. *Coord. Chem. Rev.* **2009**, *253*, 2493–2514.

(15) Kershaw Cook, L. J.; Mohammed, R.; Sherborne, G.; Roberts, T. D.; Alvarez, S.; Halcrow, M. A. Spin State Behaviour of Iron(II)/Dipyrazolylpyridine Complexes. New Insights from Crystallographic and Solution Measurements. *Coord. Chem. Rev.* **2015**, *289–290*, 2–12.

(16) Craig, G. A.; Roubeau, O.; Aromí, G. Spin State Switching in 2,6-Bis(pyrazol-3-yl)pyridine (3-bpp) Based Fe(II) Complexes. *Coord. Chem. Rev.* **2014**, *269*, 13–31.

(17) Kershaw Cook, L. J.; Kulmaczewski, R.; Mohammed, R.; Dudley, S.; Barrett, S. A.; Little, M. A.; Deeth, R. J.; Halcrow, M. A. A Unified Treatment of the Relationship Between Ligand Substituents and Spin State in a Family of Iron(II) Complexes. *Angew. Chem. Int. Ed.* **2016**, *55*, 4327–4331.

(18) Pavlik, J.; Linares, J. Microscopic Models of Spin Crossover. *C. R. Chimie* **2018**, *21*, 1170–1178.

(19) (a) Palii, A.; Ostrovsky, S.; Reu, O.; Tsukerblat, B.; Decurtins, S.; Liu, S.-X.; Klokishner, S. Microscopic Theory of Cooperative Spin Crossover: Interaction of Molecular Modes with Phonons. *J. Chem. Phys.* **2015**, *143*, 084502/1–12. (b) Parpiiev, T.; Servol, M.; Lorenc, M.; Chaban, I.; Lefort, R.; Collet, E.; Cailleau, H.; Ruello, P.; Daro, N.; Chastanet, G.; Pezeril, T.

Ultrafast Non-Thermal Laser Excitation of Gigahertz Longitudinal and Shear Acoustic Waves in Spin-Crossover Molecular Crystals [Fe(PM-AzA)$_2$(NCS)$_2$]. *Appl. Phys. Lett.*, **2017**, *111*, 151901/1–5. (c) Collet, E.; Azzolina, G.; Ichii, T.; Guerin, L.; Bertoni, R.; Moréac, A.; Cammarata, M.; Daro, N.; Chastanet, G.; Kubicki, J.; Tanaka, K.; Matar, S. F. Lattice Phonon Modes of the Spin Crossover Crystal [Fe(phen)$_2$(NCS)$_2$] Studied by THz, IR, Raman Spectroscopies and DFT Calculations. *Eur. Phys. J. B* **2019**, *92*, 12/1–10.

(20) SIGMAPLOT v 8.02, SPSS Inc., 2002.

(21) Groom, C. R.; Bruno, I. J.; Lightfoot, M. P.; Ward, S. C. The Cambridge Structural Database. *Acta Cryst. Sect. B Struct. Sci. Cryst. Eng. Mater.* **2016**, *72*, 171–179.

(22) (a) Evans, D. F. The Determination of the Paramagnetic Susceptibility of Substances in Solution by Nuclear Magnetic Resonance. *J. Chem. Soc.* **1959**, 2003–2005. (b) Schubert, E. M. Utilizing the Evans Method with a Superconducting NMR Spectrometer in the Undergraduate Laboratory. *J. Chem. Educ.* **1992**, *69*, 62.

(23) O'Connor, C. J. Magnetochemistry – Advances in Theory and Experimentation. *Prog. Inorg. Chem.* **1982**, *29*, 203–283.

(24) García, B.; Ortega, J. C. Excess Viscosity η^E, Excess Volume V^E, and Excess Free Energy of Activation ΔG^{*E} at 283, 293, 303, 313, and 323 K for Mixtures of Acetonitrile and Alkyl Benzoates. *J. Chem. Eng. Data* **1988**, *33*, 200−204**.**

(25) Sugiyarto, K. H.; Scudder, M. L.; Craig, D. C.; Goodwin, H. A. Electronic and Structural Properties of the Spin Crossover Systems Bis(2,6-bis(pyrazol-3-yl)pyridine)iron(II) Thiocyanate and Selenocyanate. *Aust. J. Chem.* **2000**, *53*, 755−765.

(26) Table 1 includes $[Fe(3\text{-}bpp)_2][NCS]_2$ (Chart 1), which we newly characterized during this study. This was originally reported as its dihydrate phase $[Fe(3\text{-}bpp)_2][NCS]_2 \cdot 2H_2O$, whose SCO occurs in two unequal steps.[25] The form of this transition is sample-dependent, and repeated thermal cycling about $T_{½}$ caused a reversible transformation of the material to a new phase exhibiting abrupt SCO in one step ($T_{½}$ = 230 K). These aged samples have a different powder pattern from the freshly prepared material, and were attributed to a second, metastable phase of the hydrated complex.[68] However, comparison of anhydrous $[Fe(3\text{-}bpp)_2][NCS]_2$ with these literature data implies that the reversible phase change instead corresponds to a facile dehydration and rehydration of the material under ambient conditions (Figure S14).

(27) Barrett, S. A.; Kilner, C. A.; Halcrow, M. A. Spin-Crossover in $[Fe(3\text{-}bpp)_2][BF_4]_2$ in Different Solvents – a Dramatic Stabilisation of the Low-Spin State in Water. *Dalton Trans.* **2011**, *40*, 12021–12024.

(28) Jeon, I.-R.; Park, J. G.; Haney, C. R.; Harris, T. D. Spin Crossover Iron(II) Complexes as PARACEST MRI Thermometers. *Chem. Sci.* **2014**, *5*, 2461–2465.

(29) Bartual-Murgui, C.; Vela, S.; Darawsheh, M.; Diego, R.; Teat, S. J.; Roubeau, O.; Aromí, G. A Probe of Steric Ligand Substituent Effects on the Spin Crossover of Fe(II) Complexes. *Inorg. Chem. Front.* **2017**, *4*, 1374–1383.

(30) Dance, I.; Scudder, M. Molecules Embracing in Crystals. *CrystEngComm* **2009**, *11*, 2233–2247.

(31) Pritchard, R.; Kilner, C. A.; Halcrow, M. A. Iron(II) Complexes with a Terpyridine Embrace Packing Motif Show Remarkably Consistent Cooperative Spin-Transitions. *Chem. Commun.* **2007**, *2007*, 577–579.

(32) Kershaw Cook, L. J.; Shepherd, H. J.; Comyn, T. P.; Baldé, C.; Cespedes, O.; Chastanet, G.; Halcrow, M. A. Decoupled Spin-Crossover and Structural Phase Transition in a Molecular Iron(II) Complex. *Chem. Eur. J.* **2015**, *21*, 4805–4816.

(33) Kershaw Cook, L. J.; Kulmaczewski, R.; Cespedes, O.; Halcrow, M. A. Different Spin State Behaviors in Isostructural Solvates of a Molecular Iron(II) Complex. *Chem. Eur. J.* **2016**, *22*, 1789–1799.

(34) Guionneau, P.; Marchivie, M.; Bravic, G.; Létard, J.-F.; Chasseau, D. Structural Aspects of Spin Crossover. Example of the $[Fe^{II}L_n(NCS)_2]$ Complexes. *Top. Curr. Chem.* **2004**, *234*, 97–128.

(35) Capel Berdiell, I.; Kulmaczewski, R.; Halcrow, M. A. Iron(II) Complexes of 2,4-Dipyrazolyl-1,3,5-triazine Derivatives – the Influence of Ligand Geometry on Metal Ion Spin state. *Inorg. Chem.* **2017**, *56*, 8817−8828.

(36) McCusker, J. K.; Rheingold, A. L.; Hendrickson, D. N. Variable-Temperature Studies of Laser-Initiated $^5T_2 \rightarrow {}^1A_1$ Intersystem Crossing in Spin-Crossover Complexes: Empirical Correlations between Activation Parameters and Ligand Structure in a Series of Polypyridyl Ferrous Complexes. *Inorg. Chem.* **1996**, *35,* 2100−2112.

(37) Average Σ and Θ values for $[Fe(1\text{-bpp})_2]^{2+}$ derivatives are 160 and 486° (high-spin), or 88 and 284° (low-spin). Corresponding values for $[Fe(3\text{-bpp})_2]^{2+}$ are 148 and 470° (high-spin), or 97 and 313° (low-spin). These averages were calculated from the tabulated data in refs. 10, 14 and 16.

(38) Šalitroš, I.; Fuhr, O.; Eichhöfer, A.; Kruk, R.; Pavlik, J.; Dlháň, L.; Boča, R.; Ruben, M. The Interplay of Iron(II) Spin Transition and Polymorphism. *Dalton Trans.* **2012**, *41*, 5163–5171.

(39) Kulmaczewski, R.; Trzop, E.; Kershaw Cook, L. J.; Collet, E.; Chastanet, G.; Halcrow, M. A. Role of Symmetry Breaking in the Structural Trapping of Light-Induced Excited Spin States. *Chem. Commun.* **2017**, *53*, 13268–13271.

(40) Money, V. A.; Carbonera, C.; Elhaïk, J.; Halcrow, M. A.; Howard, J. A. K.; Létard, J.-F. Interplay Between Kinetically Slow Thermal Spin-Crossover and Metastable High-Spin State Relaxation in an Iron(II) Complex with Similar $T_{½}$ and T(LIESST). *Chem. Eur. J.* **2007**, *13*, 5503–5514.

(41) See *eg* (a) Tovee, C. A.; Kilner, C. A.; Barrett, S. A.; Thomas, J. A.; Halcrow, M. A. A Back-to-back Ligand with Dipyrazolylpyridine and Dipicolylamine Metal-Binding Domains. *Eur. J. Inorg. Chem.* **2010**, *2010*, 1007–1012. (b) Takahashi, K.; Hasegawa, Y.; Sakamoto, R.; Nishikawa, M.; Kume, S.; Nishibori, E.; Nishihara, H. Solid-State Ligand-Driven Light-Induced Spin Change at Ambient Temperatures in Bis(dipyrazolylstyrylpyridine)iron(II) Complexes. *Inorg. Chem.* **2012**, *51*, 5188−5198. (c) Schäfer, B.; Bauer, T.; Faus, I.; Wolny, J. A.; Craig, G. A.; Costa, J. S.; Teat, S. J.; Roubeau, O.; Yufit, D. S.; Howard, J. A. K.; Aromí, G. Multimetastability in a Spin-Crossover Compound Leading to Different High-Spin-to-Low-Spin Relaxation Dynamics. *Inorg. Chem.* **2013**, *52*, 7203−7209. (d) Dahms, F.; Fuhr, O.; Lebedkin, S.; Wille, H.-C.; Schlage, K.; Chevalier, K.; Rupp, F.; Diller, R.; Schünemann, V.; Kappes, M. M.; Ruben, M. A Luminescent Pt_2Fe Spin Crossover Complex. *Dalton Trans.* **2017**, *46*, 2289–2302.

(42) (a) Ritter, G.; König, E.; Irler, W.; Goodwin, H. A. The High-Spin ($^5T_2$) ↔ Low-Spin ($^1A_1$) Transition in Solid Bis[2-(2-pyridylamino)-4-(2-pyridyl)thiazole]iron(II) Dinitrate. Its Dependence on Time and on the Previous History of the Specimen. *Inorg. Chem.* **1978**, *17*, 224–228. (b) Létard, J.-F.; Asthana, S.; Shepherd, H. J.; Guionneau, P.; Goeta, A. E.; Suemura, N.; Ishikawa, R.; Kaizaki, S. Photomagnetism of a *sym-cis*-Dithiocyanato Iron(II) Complex with a Tetradentate *N*,*N*'-Bis(2-pyridylmethyl)1,2-ethanediamine Ligand. *Chem. Eur. J.* **2012**, *18*, 5924–5934. (c) Paradis, N.; Chastanet, G.; Varret, F.; Létard, J.-F. Metal Dilution of Cooperative Spin-Crossover Compounds: When Stable and Metastable High-Spin States Meet. *Eur. J. Inorg. Chem.* **2013**, *2013*, 968–974.

(43) Holland, J. M.; McAllister, J. A.; Kilner, C. A.; Thornton-Pett, M.; Bridgeman, A. J.; Halcrow, M. A. Stereochemical Effects on the Spin-State Transition Shown by Salts of $[FeL_2]^{2+}$ [L = 2,6-Di(pyrazol-1-yl)pyridine]. *J. Chem. Soc. Dalton Trans.* **2002**, *2002,* 548–554.

(44) Kershaw Cook, L. J.; Thorp-Greenwood, F. L.; Comyn, T. P.; Cespedes, O.; Chastanet, G.; Halcrow, M. A. Unexpected Spin-Crossover and a Low Pressure Phase Change in an Iron(II)/Dipyrazolylpyridine Complex Exhibiting a High-Spin Jahn-Teller Distortion. *Inorg. Chem.* **2015**, *54*, 6319–6330.

(45) Kumar, K. S.; Heinrich, B.; Vela, S.; Moreno-Pineda, E.; Bailly, C.; Ruben, M. Bi-stable Spin-Crossover Characteristics of a Highly Distorted $[Fe(1\text{-BPP-}COOC_2H_5)_2](ClO_4)_2\cdot CH_3CN$ Complex. *Dalton Trans.* **2019**, *48*, 3825–3830.

(46) Vela, S.; Novoa, J. J.; Ribas-Arino, J. Insights into the Crystal-Packing Effects on the Spin Crossover of $[Fe^{II}(1\text{-bpp})_2]^{2+}$-Based Materials. *Phys. Chem. Chem. Phys.* **2014**, *16*, 27012–27024.

(47) (a) Létard, J.-F.; Guionneau, P.; Codjovi, E.; Lavastre, O.; Bravic, G.; Chasseau, D.; Kahn, O. Wide Thermal Hysteresis for the Mononuclear Spin-Crossover Compound *cis*-Bis(thiocyanato)bis[*N*-(2'-pyridylmethylene)-4-(phenylethynyl)anilino]iron(II). *J. Am. Chem. Soc.* **1997**, *119*, 10861–10862. (b) Guionneau, P.; Létard, J.-F.; Yufit, D. S.; Chasseau, D.; Bravic, G.; Goeta, A. E.; Howard, J. A. K.; Kahn, O. Structural Approach of the Features of the Spin Crossover Transition in Iron(II) Compounds. *J. Mater. Chem.* **1999**, *9*, 985–994. (c) Létard, J.-F.; Chastanet, G.; Nguyen, O.; Marcén, S.; Marchivie, M.; Guionneau, P.; Chasseau, D.; Gütlich, P. Spin Crossover Properties of the $[Fe(PM\text{-}BiA)_2(NCS)_2]$ Complex – Phases I and II. *Monatsh. Chem.* **2003**, *134*, 165–182. (d) Létard, J.-F.; Kollmansberger, M.; Carbonera, C.; Marchivie, M.; Guionneau, P. Structural, Magnetic and Photomagnetic Study of the $[Fe(PM\text{-}NEA)_2(NCS)_2]$ Spin Crossover Complex. *C. R. Chimie* **2008**, *11*, 1155–1165.

(48) Hansch, C.; Leo, A.; Taft, R. W. A Survey of Hammett Substituent Constants and Resonance and Field Parameters. *Chem. Rev.* **1991**, *91*, 165–195.

(49) Money, V. A.; Elhaïk, J.; Halcrow, M. A.; Howard, J. A. K. The Thermal and Light Induced Spin Transition in $[FeL_2](BF_4)_2$ (L = 2,6-Dipyrazol-1-yl-4-hydroxymethylpyridine). *Dalton Trans.* **2004**, *2004*, 1516–1518.

(50) Carbonera, C.; Costa, J. S.; Money, V. A.; Elhaïk, J.; Howard, J. A. K.; Halcrow, M. A.; Létard, J.-F. Photomagnetic Properties of Iron(II) Spin Crossover Complexes of 2,6-Dipyrazolylpyridine and 2,6-Dipyrazolylpyrazine Ligands. *Dalton Trans.* **2006**, *2006*, 3058–3066.

(51) Pritchard, R.; Lazar, H.; Barrett, S. A.; Kilner, C. A.; Asthana, S.; Carbonera, C.; Létard, J.-F.; Halcrow, M. A. Thermal and Light-Induced Spin-Transitions in Iron(II) Complexes of 2,6-

Bis(4-halopyrazolyl)pyridines: the Influence of Polymorphism on a Spin-Crossover Compound. *Dalton Trans.* **2009**, *2009*, 6656−6666.

(52) Mohammed, R.; Chastanet, G.; Tuna, F.; Malkin, T. L.; Barrett, S. A.; Kilner, C. A.; Létard, J.-F.; Halcrow, M. A. The Synthesis of New 2,6-Di(pyrazol-1-yl)pyrazine Derivatives, and the Spin State Behavior of their Iron(II) Complexes. *Eur. J. Inorg. Chem.* **2013**, *2013*, 819–831.

(53) Bartual-Murgui, C.; Codina, C.; Roubeau, O.; Aromí, G. A Sequential Method to Prepare Polymorphs and Solvatomorphs of $[Fe(1,3\text{-bpp})_2](ClO_4)_2 \cdot nH_2O$ (n = 0, 1, 2) with Varying Spin-Crossover Behaviour. *Chem. Eur. J.* **2016**, *22*, 12767−12776.

(54) Kershaw Cook, L. J.; Kulmaczewski, R.; Barrett, S. A.; Halcrow, M. A. Iron(II) Complexes of 4-Sulfanyl-, 4-Sulfinyl- and 4-Sulfonyl-2,6-dipyrazolylpyridine Ligands. A Subtle Interplay Between Spin-Crossover and Crystallographic Phase Changes. *Inorg. Chem. Front.* **2015**, *2*, 662–670.

(55) Madhu, N. T.; Šalitroš, I.; Schramm, F.; Klyatskaya, S.; Fuhr, O.; Ruben, M. Above Room Temperature Spin Transition in a Series of Iron(II) Bis(pyrazolyl)pyridine Compounds. *C. R. Chimie* **2008**, *11*, 1166−1174.

(56) Douib, H.; Cornet, L.; Flores Gonzalez, J.; Trzop, E.; Dorcet, V.; Gouasmia, A.; Ouahab, L.; Cador, O.; Pointillart, F. Spin-Crossover and Field-Induced Single-Molecule Magnet Behaviour in Metal(II)-Dipyrazolylpyridine Complexes. *Eur. J. Inorg. Chem.* **2018**, *2018*, 4452–4457.

(57) Nihei, M.; Tahira, H.; Takahashi, N.; Otake, Y.; Yamamura, Y.; Saito, K.; Oshio, H. Multiple Bistability and Tristability with Dual Spin-State Conversions in $[Fe(dpp)_2][Ni(mnt)_2]_2 \cdot MeNO_2$. *J. Am. Chem. Soc.* **2010**, *132*, 3553–3560.

(58) Haryono, M.; Heinemann, F. W.; Petukhov, K.; Gieb, K.; Müller, P.; Grohmann, A. Parallel Crystallization of a "Static" and a Spin- Crossover Polymorph of an Iron(II) Complex from the Same Solution. *Eur. J. Inorg. Chem.* **2009**, *2009*, 2136–2143.

(59) Abhervé, A.; Clemente-León, M.; Coronado, E.; Gómez-García, C. J.; López-Jordà, M. A Spin-Crossover Complex Based on a 2,6-Bis(pyrazol-1-yl)pyridine (1-bpp) Ligand Functionalized with a Carboxylate Group. *Dalton Trans.* **2014**, *43*, 9406–9409.

(60) García-López, V.; Palacios-Corella, M.; Abhervé, A.; Pellicer-Carreño, I.; Desplanches, C.; Clemente-León, M.; Coronado, E. Spin-Crossover Compounds Based on Iron(II) Complexes of 2,6-Bis(pyrazol-1-yl)pyridine (bpp) Functionalized with Carboxylic Acid and Ethyl Carboxylic Acid. *Dalton Trans.* **2018**, *47*, 16958–16968.

(61) Galadzhun, I.; Kulmaczewski, R.; Cespedes, O.; Yamada, M.; Yoshinari, N.; Konno, T.; Halcrow, M. A. 2,6-Di(pyrazolyl)pyridine-4-carboxylate Esters with Alkyl Chain Substituents, and Their Iron(II) Complexes. *Inorg. Chem.* **2018**, *57*, 13761–13771.

(62) Attwood, M.; Akutsu, H.; Martin, L.; Cruickshank, D.; Turner, S. S. Above Room Temperature Spin Crossover in Thioamide-Functionalised 2,6-Bis(pyrazol-1-yl)pyridine Iron(II) Complexes. *Dalton Trans.* **2019**, *48*, 90–98.

(63) Hasegawa, Y.; Sakamoto, R.; Takahashi, K.; Nishihara, H. Bis[(*E*)‑2,6-bis(1H‑pyrazol-1-yl)-4-styrylpyridine]iron(II) Complex: Relationship between Thermal Spin Crossover and Crystal Solvent. *Inorg. Chem.* **2013**, *52*, 1658–1665.

(64) Šalitroš, I.; Fuhr, O.; Kruk, R.; Pavlik, J.; Pogány, L.; Schäfer, B.; Tatarko, M.; Boča, R.; Linert, W.; Ruben, M. Thermal and Photoinduced Spin Crossover in a Mononuclear Iron(II) Complex with a Bis(pyrazolyl)pyridine Type of Ligand. *Eur. J. Inorg. Chem.* **2013**, *2013*, 1049–1057.

(65) Šalitroš, I.; Pavlik, J.; Boča, R.; Fuhr, O.; Rajadurai, C.; Ruben, M. Supramolecular Lattice-Solvent Control of Iron(II) Spin Transition Parameters. *CrystEngComm* **2010**, *12*, 2361–2368.

(66) Elhaïk, J.; Money, V. A.; Barrett, S. A.; Kilner, C. A.; Evans, I. R.; Halcrow, M. A. The Spin-States and Spin-Crossover Behaviour of Iron(II) Complexes of 2,6-Dipyrazol-1-ylpyrazine Derivatives. *Dalton Trans.* **2003**, *2003*, 2053–2060.

(67) Sugiyarto, K. H.; McHale, W.-A.; Craig, D. C.; Rae, A. D.; Scudder, M. L.; Goodwin, H. A. Spin Transition Centres Linked by the Nitroprusside Ion. The Cooperative Transition in Bis(2,6-Bis(pyrazol-3-yl)pyridine)iron(II) Nitroprusside. *Dalton Trans.* **2003**, *2003*, 2443–2448.

(68) (a) Bhattacharjee, A.; Ksenofontov, V.; Sugiyarto, K. H.; Goodwin, H. A.; Gütlich, P. Anomalous Spin Transition Observed in Bis(2,6-bis(pyrazol-3-yl)pyridine)iron(II) Thiocyanate Dihydrate. *Adv. Funct. Mater.* **2003**, *13*, 877–882. (b) Bhattacharjee, A.; Kusz, J.; Ksenofontov, V.; Sugiyarto, K. H.; Goodwin, H. A.; Gütlich, P. X-Ray Powder Diffraction and LIESST-Effect of the Spin Transition Material $[Fe(bpp)_2](NCS)_2 \cdot 2H_2O$. *Chem. Phys. Lett.* **2006**, *431*, 72–77. (c) Bhattacharjee, A.; Kusz, J.; Zubko, M.; Goodwin, H. A.; Gütlich, P. Synchrotron Powder-

Diffraction Study of the Spin Transition Compound $[Fe(bpp)_2](NCS)_2 \cdot 2H_2O$ and Soft X-Ray-Induced Structural Phase Conversion. *J. Mol. Struct.* **2008**, *890*, 178–183.